

Modeling and finite element analysis of rod and wire steel rolling process

Shulun Liao^{1,2)}, Liwen Zhang^{1,2)}, Siyu Yuan^{1,2)}, Yu Zhen³⁾, and Shuqi Guo³⁾

1) School of Materials Science and Engineering, Dalian University of Technology, Dalian 116023, China

2) State Key Laboratory of Materials Modification by Laser, Ion, and Electron Beams, Dalian University of Technology, Dalian 116023, China

3) Dongbei Special Steel Group, Dalian 116031, China

(Received 2007-07-30)

Abstract: Two thermomechanical coupled elastic-plastic finite element (FE) models were developed for predicting the 12-pass continuous rolling process of GCr15 rod and wire steel. The distances between stands in the proposed models were set according to the actual values, and the billets were shortened in the models to reduce the calculation time. To keep the continuity of simulation, a technique was developed to transfer temperature data between the meshes of different models in terms of nodal parameters by interpolation functions. The different process variables related to the rolling process, such as temperature, total equivalent plastic strain, equivalent plastic strain rate, and contact friction force, were analyzed. Also, the proposed models were applied to analyze the reason for the occurrence of an excessive spread in width. Meanwhile, it was also utilized to assess the influence of the roll diameter change on the simulated results such as temperature and rolling force. The simulated results of temperature are found to agree well with the measured results.

© 2008 University of Science and Technology Beijing. All rights reserved.

Key words: width spread; rod rolling; wire rolling; temperature; rolling force; numerical simulation

[This study was supported by the Excellent Youth and Science & Technology Talent Foundation of Dalian (No.2001-122) and Dongbei Special Steel Group.]

1. Introduction

Significant progress has been made in predicting the thermomechanical parameters during hot rolling of materials to control the mechanical properties of the products as well as to control the dimension tolerances. Most of the previous studies, however, have concentrated on the modeling of the strip (or plate) rolling process [1-4]. There were also some studies on ring rolling or shape rolling [5-9], with little research carried out on the three-dimensional modeling of rod and wire multipass rolling. It was difficult to describe the rod and wire continuous rolling process using two-dimensional models because of the complex contact occurring between the rolls and billet and the three-dimensional nature of the problem. These studies on the three-dimensional modeling of rod and wire rolling mainly focused on the simulation of simple pass rolling such as single pass or double pass rolling [10-14]. For example, Li *et al.* [12] predicted the de-

formation behavior of a billet during the oval pass rolling. Considering the computational time caused by a large number of passes and the large distance between the two passes, it was difficult to develop a multipass model for rod and wire continuous rolling in terms of the actual distances between stands. Therefore, Wang *et al.* [15] shortened the distances between stands in their model and simulated the deformation of the workpiece in a four-pass bar continuous rolling process to reduce the computation time. Hong *et al.* [16] simulated the two-pass and four-pass rolling process using three-dimensional models in which the distances between stands were assumed to be short.

In the present study, with the aid of the commercial software MSC.Marc, three-dimensional models were developed to model the 12-pass rod and wire continuous rolling process by means of a shortening billet instead of the distances between stands and adopting a data transfer technique. Some variables related to the

rod and wire rolling process are investigated in this article, and they are applied to analyze the formation of the undesired shape of the billet as well as to evaluate the effect of the roll diameter on process variables. This study makes it feasible for the three-dimensional modeling of the multipass rod-wire continuous rolling process with a long rolling line, and it can be used as an offline guideline for evaluating an industrial hot rolling line.

2. Formulation of thermal-mechanical coupled FEM

Rolling is a deformation process with a transient temperature change. The elements undergo elastic and plastic change. In a nonlinear stress analysis problem, Marc carries out the analysis incrementally and expresses the governing equation in an incremental form in terms of the incremental displacement vector $\Delta \mathbf{u}$ and the incremental force vector $\Delta \mathbf{F}_p$.

$$[\mathbf{K}]\{\Delta \mathbf{u}\} = \{\Delta \mathbf{F}_p\} \quad (1)$$

where $[\mathbf{K}]$ is the elastic-plastic stiffness matrix, $\Delta \mathbf{u}$ is the incremental displacement vector, and $\Delta \mathbf{F}_p$ is the incremental force vector.

$$[\mathbf{K}] = \sum_e {}^\tau \mathbf{K}_{ep}^e = \sum_e \int_{V_e} \mathbf{B}^T {}^\tau \mathbf{D}_{ep} \mathbf{B} dV \quad (2)$$

$$\{\Delta \mathbf{F}_p\} = \sum_e {}^{t+\Delta t} \mathbf{Q}_i^e - \sum_e {}^t \mathbf{Q}_i^e \quad (3)$$

$${}^{t+\Delta t} \mathbf{Q}_i^e = \int_{V_e} \mathbf{N}^T {}^{t+\Delta t} \bar{\mathbf{F}} dV + \int_{S_e} \mathbf{N}^T {}^{t+\Delta t} \bar{\mathbf{T}} dS \quad (4)$$

$${}^t \mathbf{Q}_i^e = \int_{V_e} \mathbf{B}^T {}^t \boldsymbol{\sigma} dV \quad (5)$$

where e is the element number, ${}^\tau \mathbf{K}_{ep}^e$ the elastic-plastic stiffness matrix of the element at time τ , \mathbf{B} the geometric matrix, ${}^\tau \mathbf{D}_{ep}$ the elastic-plastic matrix at time τ , ${}^{t+\Delta t} \mathbf{Q}_i^e$ the exterior load vector at time $t + \Delta t$, ${}^t \mathbf{Q}_i^e$ the interior load vector at time t , \mathbf{N} the shape function, ${}^{t+\Delta t} \bar{\mathbf{F}}$ the load vector in volume V_e at time $t + \Delta t$, V_e the element volume, ${}^{t+\Delta t} \bar{\mathbf{T}}$ the load vector on the boundary S_e at time $t + \Delta t$, S_e the stress boundary of the element, and ${}^t \boldsymbol{\sigma}$ the stress vector at time t .

The three-dimensional FEM format of the temperature field equation can be deduced as:

$$[\mathbf{K}_T]\{\mathbf{T}\} + [\mathbf{C}]\{\dot{\mathbf{T}}\} = \{\mathbf{P}\} \quad (6)$$

where $[\mathbf{K}_T]$ is the conductivity matrix, $[\mathbf{C}]$ the heat capacity matrix, $\{\mathbf{P}\}$ the heat flow vector, $\{\mathbf{T}\}$ the nodal temperature matrix, and $\{\dot{\mathbf{T}}\}$ the differential coefficient matrix of nodal temperature to time.

The transient temperature field can be obtained by solving this large equation group.

$$[\mathbf{K}_T] = \sum_e \int_{V_e} \mathbf{B}^T {}^\tau \mathbf{D}_{ep} \mathbf{B} dV \quad (7)$$

$$\mathbf{C}_{ij} = \sum_e \mathbf{C}_{ij}^e = \sum_e \int_{\Omega^e} \rho c N_i N_j d\Omega \quad (8)$$

$$\mathbf{P}_i = \sum_e \mathbf{P}_{Q_i}^e + \sum_e \mathbf{P}_{q_i}^e + \sum_e \mathbf{P}_{h_i}^e = \sum_e \int_{\Omega^e} \rho Q N_i d\Omega + \sum_e \int_{\Gamma_2^e} q N_i d\Gamma + \sum_e \int_{\Gamma_3^e} h \phi_a N_i d\Gamma \quad (9)$$

where \mathbf{B} is the geometric matrix, \mathbf{C}_{ij} the total heat capacity matrix, \mathbf{C}_{ij}^e the heat capacity matrix of the element, ρ the density, c the specific heat, N_i and N_j are the shape function, Ω^e is the zone of the inner element, \mathbf{P}_i the row matrix of the total thermal load, $\mathbf{P}_{Q_i}^e$ the row matrix of thermal load of the inner element, $\mathbf{P}_{q_i}^e$ the row matrix of thermal load of the flux boundary element, and $\mathbf{P}_{h_i}^e$ the row matrix of thermal load of the convection boundary element, Q the heat flux density of the inner element, q the flux density on the element flux boundary Γ_2^e , h the natural convection exchange coefficient, Γ_3^e the element natural convection boundary, ϕ_a the temperature of surroundings.

Combining Eq. (1) with Eq. (6), the following equation will be obtained:

$$\begin{bmatrix} [0] & [0] \\ [0] & [\mathbf{C}] \end{bmatrix} \begin{Bmatrix} \{\dot{\mathbf{u}}\} \\ \{\dot{\mathbf{T}}\} \end{Bmatrix} + \begin{bmatrix} [\mathbf{K}] & [0] \\ [0] & [\mathbf{K}_T] \end{bmatrix} \begin{Bmatrix} \{\mathbf{u}\} \\ \{\mathbf{T}\} \end{Bmatrix} = \begin{Bmatrix} \{\mathbf{F}\} \\ \{\mathbf{P}\} \end{Bmatrix} \quad (10)$$

where $\{\dot{\mathbf{u}}\}$ is the vector of velocity, $\{\mathbf{u}\}$ the displacement vector, and $\{\mathbf{F}\}$ the force vector.

In coupled analysis, the temperature field and deformation can be solved in terms of iterative ways according to the FE equation above.

3. Modeling

3.1. FE model

Dongbei Special Steel Group has imported a block with a 30-stand continuous rod and wire production line with temperature control facilities. The mill assignment of the front 12 passes is represented schematically in Fig. 1. The GCr15 square billets of 150 mm × 150 mm are passed through the 12 passes and rolled into a rod-wire with a radius of 16 mm. The rolling line length is extremely large compared with the billet thickness. Therefore, the whole rolling process is described using two FE models based on the commercial software MSC.Marc. In the two models,

the billet is defined as a deformation body and the rolls are defined as rigid bodies. Owing to the symmetry of billet and rolls, a quarter of the billet and rolls was included in the geometric model. Fig. 2 shows the first model, which includes the descaling stage and rough rolling stands. The x , y , and z axes in the model represent the directions of rolling, thickness, and width, respectively. The total element number of the billet is 1035 and the total node number is 1392. The length of the billet is 400 mm and the distance between the two stands is 2600 mm. The quasi static analysis is adopted in the simulation of the first model. A rigid body whose speed is controlled by MSC.Marc's subroutine is employed to stick to the end of the billet, so it can push the billet to the entry of the next stand with a slight force and an actual exit speed during the inter-pass time. The method has also been employed in the static analysis of the second model, which is similar to the first model, but also has differences, such as the shape and dimension of rolls and billet, the distances between stands, and rolling speed. The second model includes the cooling process on the conveyor and the first section of intermediate stands. Fig. 3 shows the second model in which the length of the billet is 300 mm and the distance between the two stands is 2500 mm. The total element number is 2730, and the total node number is 3621.

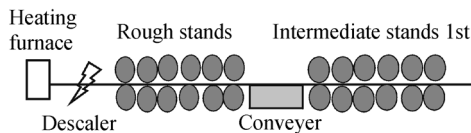


Fig. 1. Mill layout of rolling mills.

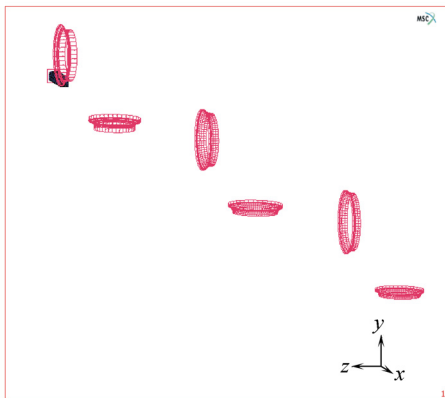


Fig. 2. FE model of the rough rolling process.

3.2. Simulation condition

The friction is a complex physical phenomena on account of the variations in surface conditions, relative sliding, temperature, geometry, and so on. Marc allows users to define the friction model by means of using its UFRIC subroutine. The friction coefficient is obtained as

$$\mu = \theta_1 \cdot \theta_2 \cdot \theta_3 \cdot (1.05 - 0.0005\theta) \quad (11)$$

where θ is the temperature of the contact surface, θ_1 and θ_3 are the modifying factors determined by different rolls and steels, respectively. $\theta_2 = 0.4 + 0.6e^{-0.2(v-2.0)}$, it is determined by the rolling speed.

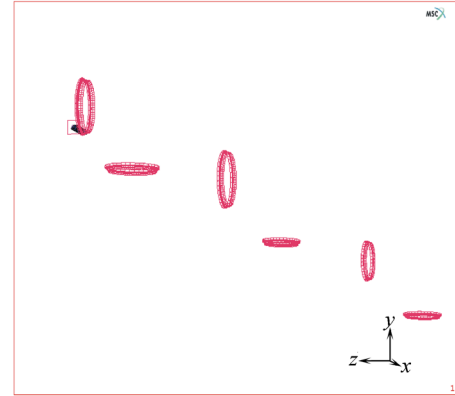


Fig. 3. FE model of the mid-rolling process.

The heat generated by friction is fairly assigned to the rolls and billet. The deformation of the billet will generate heat, and 90% of the power of deformation is transformed into heat. On the symmetrical surface of the billet, it is supposed that the heat flux is 0. And the main parameters adopted in the two models are shown in Table 1.

Table 1. Thermal conditions used in the analysis

Initial temperature of material / °C	1045
Temperature of roll / °C	100
Heat transfer coefficient from roll to material / (kW·m ⁻² ·K ⁻¹)	9.5
Emission and convection coefficient from material to surroundings / (kW·m ⁻² ·K ⁻¹)	0.07
Atmospheric temperature / °C	20

4. Data transfer technique

Because of the limitation of the current computer speed, the whole rolling process was described with two three-dimensional models. To keep the continuity of simulation, the temperature results of the first model should be inherited as the initial conditions of the second model. Therefore, a procedure for data transfer with the aid of MSC.Marc and its subroutines to accomplish the process is developed in this article.

The data transfer technique consists of three parts. The first is to extract the output data of the first model including nodal temperature, nodal coordinates, Gaussian point coordinates, element number, and nodal displacements. The second is to judge the relationship between each node in the second model and the elements in the first model and to solve the nodal tem-

peratures of the second model by means of data mapping. The third is to feed the temperature results into the new model as an initial condition of calculation with Marc's subroutine USINC. Fig. 4 shows a schematic diagram of data mapping. As shown in Fig. 4(a), there is a final mesh with a large deformation after six rolling passes. Fig. 4(b) shows an entirely new mesh, which has the same shape and dimension in cross-section as the one in Fig. 4(a). With assumptions of accuracy, it is necessary to employ a new mesh, which is shortened so as to reduce the computational time. When the final mesh in Fig. 4(a) is replaced by the new mesh in Fig. 4(b), the temperature values of all nodes in the new mesh need to be determined according to the temperature results of the final mesh. The new mesh can be regarded as a part of the final mesh in Fig. 4(a), and then there exists a connection that each node in the new mesh will locate inside some elements of the final mesh in Fig. 4(a). In the proposed models, the billet is modeled as an elastic-plastic object using an eight-node isoparametric hexahedron element that uses eight-point Gaussian integration. If all the eight nodes of an element are determined, the element is then known. That is to say, each node of the mesh in Fig. 4(b) can be expressed by eight nodes of its related elements on the mesh in Fig. 4(a). Therefore, the temperature field values of each node in the new mesh can be determined by the related elements of the mesh in Fig. 4(a) in terms of the nodal parameters by the integration functions.

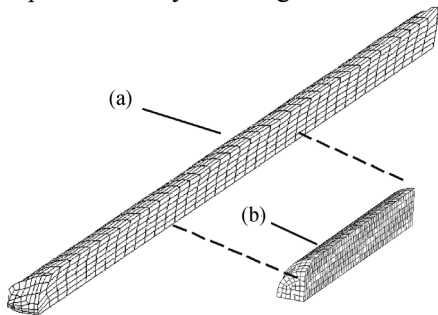


Fig. 4. Schematic diagram of the data mapping between billet meshes: (a) the final mesh in the first model; (b) the new mesh in the second model.

5. Analysis and discussion

5.1. Temperature distribution

The temperature contour of the billet at the end of rough rolling is presented in Fig. 5. During the deformation of the hot billet, the surface temperature drops rapidly because of the large temperature difference between the roll and the billet. It is observed that there is a severe temperature gradient between the surface and the center of the billet. Fig. 6 shows the initial temperature distribution of the billet in the second model calculated by the data transfer technique.

Fig. 7 shows the temperature evolution during the rolling process in some positions such as at the center of cross-section, at a depth of about one-fourth thickness, at a depth of about one-eighth thickness, and at the surface of the billet. As shown in Fig. 7, the surface temperature has a quick drop when entering the descaling zone and then returns back slowly. Because of the relatively cold rolls, the billet surface temperature drops rapidly in the roll gaps and rises slowly thereafter. With an increase in velocity, the contact time is shortened and deformation heat is increased rapidly, which results in a lower drop in surface temperature. The center temperature increases slightly in the roll gaps because of the deformation heat and decreases slowly during the inter-pass period because of the heat loss by convection and radiation. The temperature variations at the depths of about one-fourth thickness and one-eighth thickness are similar to temperature changes at the center. Whereas, the temperature drops at the depths of about one-fourth thickness and one-eighth thickness are larger than that at the center during the inter-pass period.

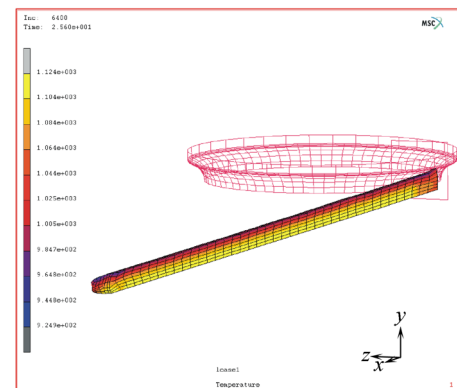


Fig. 5. Temperature contour of the billet at the end.

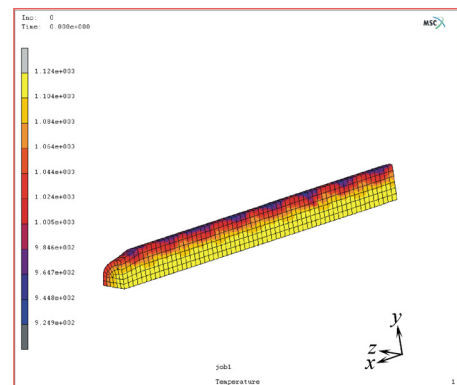


Fig. 6. Interpolation results in the second model.

5.2. Total equivalent plastic strain

Fig. 8 shows the variations of total equivalent plastic strain with time at three different positions during rough rolling. The magnitude of strain is relevant to the reduction at various passes. The highest deforma-

tion region exists near the interface of the rolls and billet, and the deformation gradually penetrates into the billet center. As shown in Fig. 8, the total strain of node a, which contacts each roll during rolling, is higher than those of node b and node c.

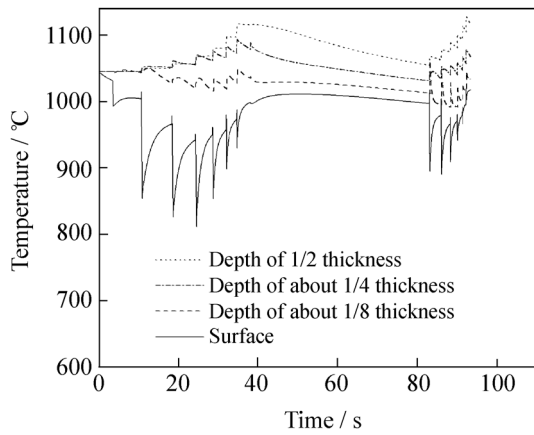


Fig. 7. Temperature profiles at different positions of the billet during rolling.

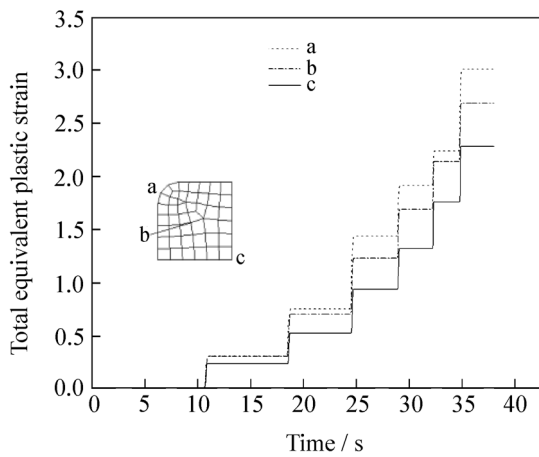


Fig. 8. History of total equivalent plastic strain at various positions during the rough rolling.

5.3. Strain rate distribution

Fig. 9 shows the equivalent plastic strain rate distribution of the billet during the first pass. From the figure, it can be seen that the nonuniformity of the strain rate in various directions is rather strong. As a result of friction, the surface of the billet experiences a higher strain rate than the center. The high equivalent plastic strain rate zone exists close to the entry of the roll gap owing to the drastic deformation there. It is very clear that the strain rate correlates positively with the speed of the billet, that is, as the rolling speed increases, the strain rate also increases.

5.4. Contact friction force

Fig. 10 shows the distribution of the contact friction component force in the x direction during the first and the seventh pass rolling. As shown in Fig. 10, the component of contact friction force is positive within

a large area at the entry of the roll gap, whilst the component of contact friction force is negative within a small region at the exit of the rolling pass. The difference shows that the friction is complex within the contact area and has large variations along the x direction. The friction force in the x direction drives the surface node into a roll gap, and then changes into a reverse direction when the node exits from the roll gap.

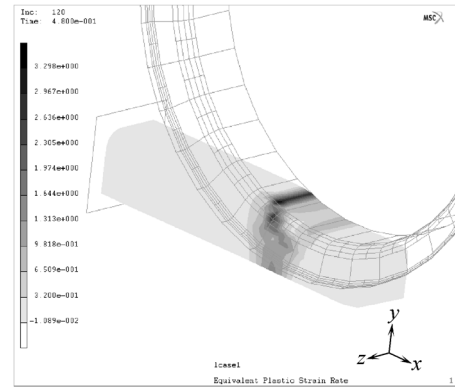


Fig. 9. Equivalent strain rate distribution during the first pass.

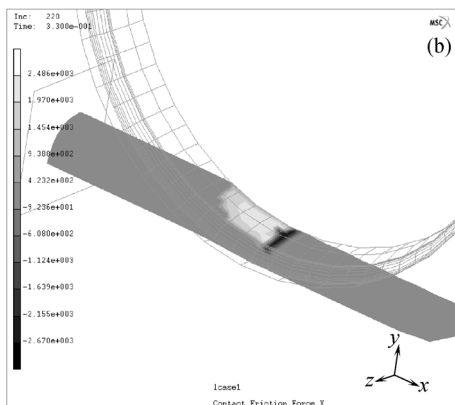
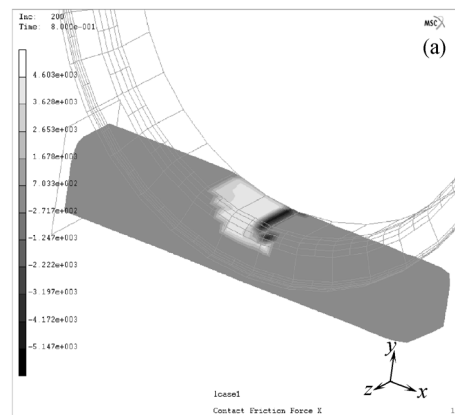


Fig. 10. Distribution of the contact friction component force: (a) the first pass; (b) the seventh pass.

5.5. Width spread

The bar with a radius of 16 mm would be formed after 12 passes rolling. The simulated grid shapes of the billet after the eleventh pass and twelfth pass are

illustrated in Fig. 11. Fig. 11(a) shows an excessive width spread in the vertical direction after the twelfth pass, which is often observed in practical production. The billet with the desired round shape of cross section will be obtained only by slightly increasing the roll gap in the twelfth pass compared with Fig. 11(a), as shown in Fig. 11(b). However, it is worth noting that when the roll gap is suitable in the twelfth pass, but is a bit larger in the eleventh pass, the excessive width spread will also be observed by simulation. In this case, a desired shape can be obtained through slightly shortening the roll gap in the eleventh pass.

5.6. Effect of roll diameter change on the rolling parameters

It can be observed that the roll groove shape at the stage of rough rolling has a notable change compared with the first use after a specific amount of production. To save costs and keep the dimension accuracy of billets, the roll will be machined into the one with the original roll groove shape and be used again. After several repetitions, the newly generated roll will have a great decrease in diameter when employed again. To estimate the influence of roll diameter change on the process variables, the models adopting the standard roll and the roll after reduction in roll diameter are established according to the data in Table 2. In model b, the roll groove shape and rolling speed at each pass remain unchanged, but the roll diameters adopt the actual values after reduction.

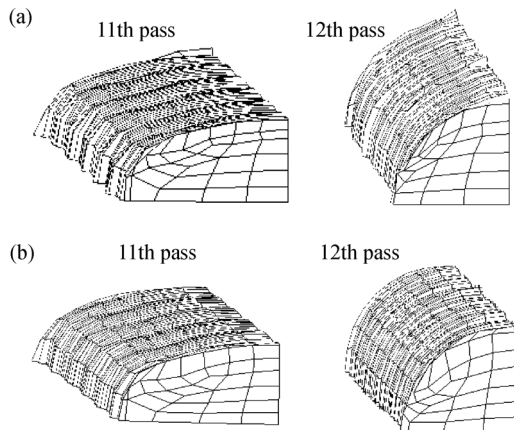


Fig. 11. Simulated shape of the billet after the eleventh pass and the twelfth pass.

Table 2. Roll diameter employed in model a and model b

	mm					
Pass	1	2	3	4	5	6
Model a	580	520	580	520	580	520
Model b	525	470	520	495	540	440

Fig. 12 shows a comparison of temperature profiles calculated by model a and model b. At the end of

rough rolling, the temperatures in model b are slightly lower than those in model a at the depth of one-fourth thickness and at the center of the billet, whilst the surface temperature in model b is slightly higher than that in model a. The difference between the two, however, is relatively little at the end of rough rolling, which is about 6–7°C. The heat of deformation is less because of the decrease in deformation power. Therefore, the inner temperature rises at the roll gap in model b is slightly lower than that in model a. The drop in the surface temperature in model b is less. This might be attributed to the reduction of the contact area between billet and rolls. Further, it should be noted that the temperature difference between the two also increases as the rolling speed increases.

The rolling force is directly affected by friction coefficient, contact area, temperature, material properties, flow stress, and so on. The reduction and roll diameter affect the rolling force indirectly by changing the contact area. The rolling force increases with time at the bite stage of rolling, and then has fluctuations within a small range at the stable stages of rolling, after which it drops at the exit stage of the billet. As only a quarter billet was modeled, the actual rolling force should be twice the average values at the stable state stages of rolling. Fig. 13 shows a comparison of the average rolling force of various passes at the stable stages of rolling in model a and model b. The reduction under various passes is 19.4%, 21.6%, 28.0%, 22.7%, 23.5%, and 24.0%, respectively. As seen in Fig. 13, the reduced roll diameter causes the rolling force to drop. It is seen that the rolling force approaches the largest value in the third pass. Furthermore, the rolling force in oval passes, such as the third and fifth pass, decreases more than in other passes.

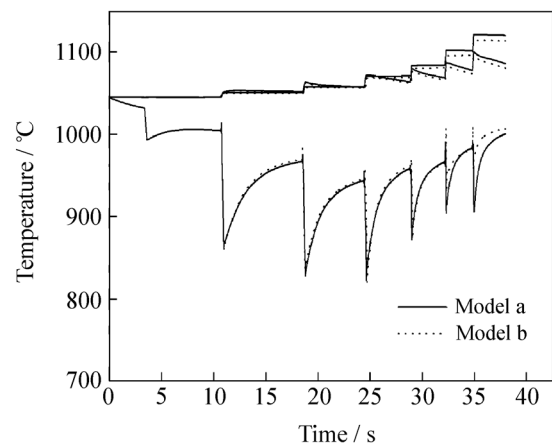


Fig. 12. Comparison of temperature profiles between model a and model b.

This analysis shows that the change of roll diameter has a slight influence on temperature variation. Nev-

ertheless, it affects the rolling force greatly, which is notable. In the case of the same reduction, the reduced roll diameter also leads to the increase in bite angle, which is disadvantageous for the billet to feed into the roll gap.

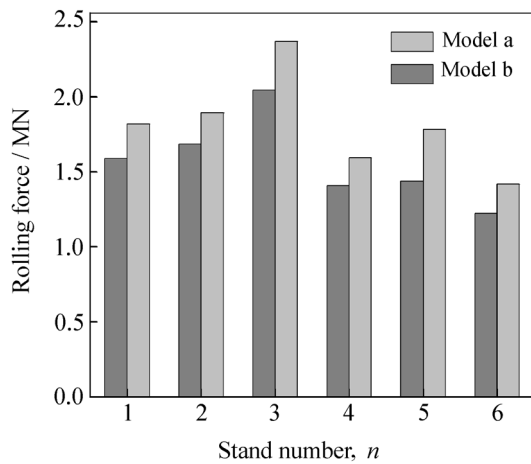


Fig. 13. Comparison of the rolling force between model a and model b.

5.7. Comparison of temperature results

To verify the proposed models, the temperature measurements were conducted on the area near the profile midline of the rolled billet by using a MIKRON-M90 handheld pyrometer. A comparison between the experimental data and the predicted results of surface temperature is presented in Fig. 14. The nodes c, b, and a on the free surface of the billet can represent the measurement area. There is a good agreement between the model predictions and experimental results, as can be seen in Fig. 14.

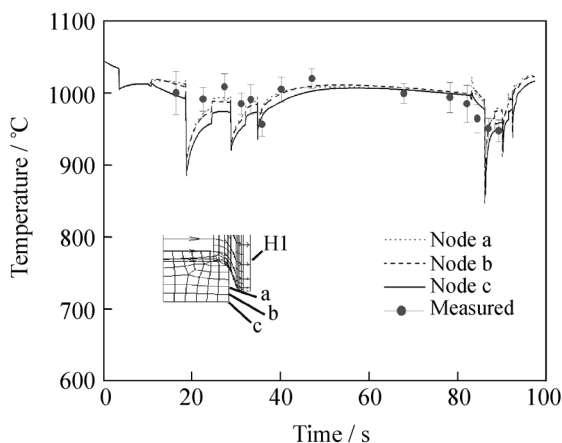


Fig. 14. Comparison between the simulated and measured values of temperature of GCr15 rod-wire.

6. Conclusions

(1) Three-dimensional models of the multipass rolling process of GCr15 rod-wire steel are developed by thermomechanical coupled elastic-plastic FEM.

The actual distances between stands and the shortened billet are adopted in the proposed models, and a data transfer technique is developed to transfer the temperature data between the meshes of different models by an integration function.

(2) The models are applied to predict the distribution of temperature, total equivalent plastic strain, strain rate, and contact friction force during rolling, and are utilized to analyze the phenomenon of excessive width spread. The models are also employed to evaluate the influence of roll diameter change on the process variables, such as temperature and rolling force, in practical production.

(3) It is shown that the simulated results are in good agreement with the measured ones of surface temperature. The study demonstrates that the proposed models are an efficient tool for optimizing schedules as well as describing the thermomechanical parameters and behavior of materials during each stage of the rod and wire manufacturing process.

References

- [1] X. Duan and T. Sheppard, Computation of substructural strengthening by the integration of metallurgical models into the finite element code, *Comput. Mater. Sci.*, 27(2003), p.250.
- [2] S.X. Zhou, An integrated model for hot rolling of steel strips, *J. Mater. Process. Technol.*, 134(2003), p.338.
- [3] C.G. Sun, H.N. Han, J.K. Lee *et al.*, A finite element model for the prediction of thermal and metallurgical behavior of trip on run-out-table in hot rolling, *ISIJ Int.*, 42(2002), No.4, p.392.
- [4] H. Furumoto, K. Yamada, and J. Yanagimoto, Effect of the number of work-roll surface division on prediction of contact length in coupled analysis of roll and strip deformation during sheet rolling, *ISIJ Int.*, 42(2002), No.4, p.736.
- [5] J.L. Song, A.L. Dowson, M.H. Jacobs, *et al.*, Coupled thermo-mechanical finite-element modeling of hot ring rolling process, *J. Mater. Process. Technol.*, 121(2002), p.332.
- [6] S.Y. Kim and Y.T. Im, Three-dimensional finite element analysis of non-isothermal shape rolling, *J. Mater. Process. Technol.*, 127(2002), p.57.
- [7] K. Komori, Simulation of deformation and temperature in caliber rolling effect of finite-element mesh in cross-section, *J. Mater. Process. Technol.*, 143-144(2003), p.367.
- [8] J. Yanagimoto, Strategic FEM simulator for innovation of rolling mill and process, *J. Mater. Process. Technol.*, 130-131(2002), p.224.
- [9] G. Fang and P. Zeng, 3D rigid-plastic finite element analysis for skew rolling process of the stepped part, *J. Mater. Sci. Technol.*, 19(2003), Suppl., p38.
- [10] Y. Lee, H.J. Kim, and S.M. Hwang, Analytic model for the prediction of mean effective strain in rod rolling proc-

- ess, *J. Mater. Sci. Technol.*, 114(2001), p.129.
- [11] Y.W. Wang and Y.L. Kang, Numerical simulation of round to oval rolling process, *Acta Metall. Sin. (Engl. Lett.)*, 13(2000), No.2, p.428.
- [12] J.C. Li, J.Z. Cui, Y.L. Ma, *et al.*, Simulation of rolling billet in oval pass by explicit dynamic elastic-plastic FEM, *J. Iron Steel Res. Int.*, 111(2004), No.12, p.30.
- [13] Y. Lee and Y.H. Kim, Approximate analysis of roll force in a round-oval-round pass rolling sequence, *J. Mater. Sci. Technol.*, 113(2001), p.124.
- [14] H.P. Hong and Y.L. Kang, Finite element analysis of rolling force and torque during hot continuous rolling of hot work steel, *J. Univ. Sci. Technol. Beijing* (in Chinese), 25(2003), No.1, p.44.
- [15] Y.W. Wang, Y.L. Kang, X.P. Ren, *et al.*, 3D FE simulation of workpiece deformation in the 4 pass bar continuous rolling process, *Mater. Sci. Technol.* (in Chinese), 7(1999), p.228.
- [16] H.P. Hong, Y.L. Kang, C.T. Feng, *et al.*, Three-dimensional thermo-mechanical coupled FEM simulation for hot continuous rolling of large-diameter mandrel bar, *J. Mater. Sci. Technol.*, 19(2003), Suppl., p.228.